Blue cadmium-free and air-fabricated quantum dot light-emitting diodes

Cite as: AIP Advances 13, 065314 (2023); doi: 10.1063/5.0152650
Submitted: 11 April 2023 • Accepted: 24 May 2023 •
Published Online: 7 June 2023

View Online Export Citation CrossMark

Paul Hänsch,[1,a] Selen Solak,[1] Hyung Seok Choi,[2] Yohan Kim,[2,b] Giovanni Ligorio,[1] Manuel Gensler,[2] Jiyong Kim,[2] Christine Boeffel,[2] Emil J. W. List-Kratochvil,[1,3] and Felix Hermerschmidt[1,b]

AFFILIATIONS

[1] Institut für Physik, Institut für Chemie, Humboldt-Universität zu Berlin, IRIS Adlershof, Zum Großen Windkanal 2, 12489 Berlin, Germany
[2] Functional Polymer Systems, Fraunhofer Institute for Applied Polymer Research IAP, Geiselbergstrasse 69, 14476 Potsdam, Germany
[3] Helmholtz-Zentrum Berlin für Materialien und Energie GmbH, Hahn-Meitner-Platz 1, 14109 Berlin, Germany

[a] **Current address:** Zernike Institute for Advanced Materials, University of Groningen, Nijenborgh 4, Groningen 9747 AG, The Netherlands.
[b] **Authors to whom correspondence should be addressed:** yohan.kim@iap.fraunhofer.de and felix.hermerschmidt@hu-berlin.de

ABSTRACT

Quantum dot (QD) materials have found increasing use in display applications because of their high color purity and fluorescence quantum yield, enabling devices with higher brightness and efficiency. However, to access large-area printing and coating methods that are carried out in ambient conditions, it is necessary to, first, move away from toxic cadmium, and second, to target materials that can be air-processed. Herein, we synthesize zinc selenide-based blue QD material and air-fabricate light-emitting diodes (LEDs) and single-carrier devices. The encapsulated devices were also measured under ambient conditions. Multi-shell-structured ZnSeTe/ZnSe/ZnS (core/shell/shell) QDs show pure deep blue/purple fluorescence emission with a high photoluminescence quantum yield of 78%. The blue QD-LED devices are fabricated in a conventional structure with bottom light emission with two electron transport materials (ZnO and ZnMgO). The QD-LED devices with ZnO electron transport layer show a maximum luminance of ~6200 cd m^{-2} at 9 V with a turn-on voltage of 3.5 V and current efficacy of 0.38 cd A^{-1}, while with ZnMgO electron transport layer, the devices show a maximum luminance of 3000 cd m^{-2} at 7 V with a turn-on voltage of 3 V and current efficacy of 0.6 cd A^{-1}. Electron-only and hole-only devices were fabricated to show and confirm the underlying charge transport mechanisms. To our knowledge, these results show for the first-time air-fabricated ZnSe-based QD-LEDs, paving the way for scaling up display applications and moving toward high-performance printed electronics.

Quantum dots (QDs) have been extensively studied for use in a range of applications such as displays,[1] solar cells,[2,3] photodetectors,[4,5] and biomedical applications.[6] Their use in electroluminescent displays is particularly interesting due to unique combinations of their intrinsic properties, e.g., the size-tunable emission wavelength for full-color RGB displays and their high photoluminescence quantum yield (PLQY). Examples of red, green, and blue QDs show that they can provide high brightness and efficiency and realize material and mechanical stability in light-emitting devices.[2,7,8] However, the first efficient QD nanocrystals mainly contained environmentally toxic cadmium (Cd).[9] Also, QD-light-emitting diodes (LEDs) based on blue QDs showed inferior photophysical properties compared to red and green QDs due to higher injection barriers for charge carriers.[10] As Cd is toxic and its use in electronic devices has been highly regulated by the European Union since 2003,[11] it is crucial to specifically study Cd-free blue QDs.

Previously, indium phosphide (InP)- and zinc selenide (ZnSe)-based QDs have been researched as Cd-free alternatives with great potential due to their favorable optical properties covering

the visible wavelength range.[12] Various studies have also focused on improving the device performance and lifetime of InP-based QD-LEDs through the optimization of QD materials and device structures.[12–14] In particular, QD-LEDs fabricated from InP/ZnSe/ZnS QDs as emitters were reported with an external quantum efficiency (EQE) of over 20%, where their calculated lifetime reached up to 1 × 10^6 h at 100 cd m^{-2}.[15] Furthermore, inkjet-printed RGB QD-LEDs with InP-based QDs also demonstrated good air-processability.[16] However, the toxicity of InP is also critical at this point. Therefore, ZnSe-based QDs remain important alternatives.

Previously, Kim *et al.* reported the first blue ZnSe-based QD-LED with an EQE over 20%, a maximum brightness of 88 900 cd m^{-2}, and a calculated lifetime of over 15 000 h at 100 cd m^{-2}.[17] However, most current lab-scale devices are produced in an inert atmosphere, and the air-processing of blue QDs, in particular, remains a critical issue, while their performance remains behind red and green QDs.[15,17,18] Therefore, to move forward to applications, new QD materials should provide the potential for printability and large-area production, which, in many cases, initially would require handling the materials in air.[16] Here, in our study, we demonstrate the synthesis of ZnSe-based blue multi-shell QDs and the fabrication of blue QD-LEDs and single-carrier (i.e., electron-only and hole-only) devices (EODs and HODs) under ambient conditions.

The multi-shell structured ZnSeTe/ZnSe/ZnS (core/shell/shell) QDs were synthesized by a hot injection method.[19] Figure 1 shows the transmission electron microscopy (TEM), x-ray diffraction (XRD) analysis, and PL and UV absorption spectra of ZnSeTe/ZnSe/ZnS QDs. In Fig. 1(a), the TEM image shows the average diameter of the QDs as 8.23 nm determined from over 200 particles. Their particle size distribution is shown in Fig. S1. In Fig. 1(b), three reflection peaks of the (111), (220), and (311) planes of zinc blende ZnTeSe cores are gradually shifted toward higher 2θ after the subsequent growth of ZnSe inner and then ZnS outer shells. This data indicate that the intended core/shell/shell structure was well synthesized without the adjunctive formation of a secondary phase. To further observe the influence of morphology of QDs on optoelectronic properties, UV–vis absorbance, PL spectrum, and PLQY were measured. The absorbance (black line) of the QD in toluene shows an onset at around 450 nm [Fig. 1(c)], and the PL spectrum of the solution (red line) shows a deep blue/purple peak emission at 436 nm with full width at half maximum (FWHM) of 20 nm. The PLQY of 98% was measured after ZnS outer shell synthesis, indicating a narrow size distribution and high quality of crystal growth of QDs as correlated with the results of TEM and XRD measurement. The PLQY remained at 78% even after multiple purification processes and the surface condition and purification process not fully optimized.

Compared to the PL of the QD solution [Fig. 1(c)], the PL peak maximum wavelength of the film sample was slightly red-shifted from 436 nm toward a longer wavelength of 443 nm, which might be attributed to a decreasing trend of interparticle spacing between QDs in the processing of the QD film. In addition, it accompanied a slight increase of full width at half maximum (FWHM) from 20 to 23 nm, which alludes to a generation of unintended aggregation and self-absorption between QDs. The resulting color coordinates for the CIE color space (Fig. S2) are x = 0.160, y = 0.035 for the solution

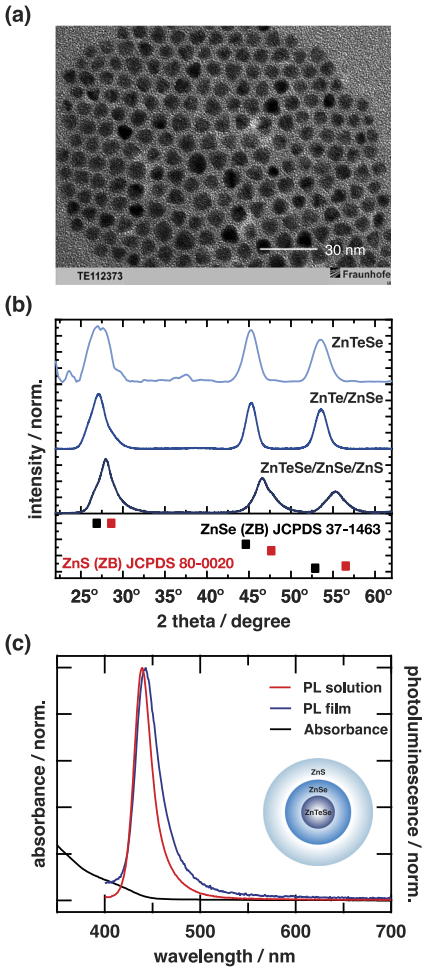

FIG. 1. (a) The TEM image shows evenly distributed ZnTeSe/ZnSe/ZnS QDs of ~8 nm size; (b) the maximum peaks of the XRD patterns of core, core/shell, and core/shell/shell are in line with the reference diffraction data of the JCPDS database; (c) UV–Vis absorbance of QDs in toluene solution (black) and photoluminescence of the QDs in solution and film (red and blue, respectively) confirm the blue emission characteristics of the material. The inset shows a schematic of the core/shell/shell architecture employed in the synthesized QDs.

and x = 0.162, y = 0.060 for the film and both lie in the deep blue region.

Having characterized the properties of the QD material itself, we air-fabricated blue QD-LEDs with TFB [poly(9,9-dioctylfluorene-alt-N-(4-sec-butylphenyl)-diphenylamine)] as hole transport and ZnO or Mg-doped ZnO (ZnMgO) nanoparticles as electron transport materials. The resulting QD-LED device has the architecture of ITO (110 nm)/PEDOT:PSS (35 nm)/TFB (7 nm)/QDs (20 nm)/ZnO or ZnMgO (50 nm)/Ag (200 nm). The Ag top electrode is vacuum deposited onto spin-coated layers and then the devices are encapsulated. A detailed description of QD synthesis and QD-LED fabrication can be found in the supplementary material.

Charge carrier imbalance, e.g., superior electron mobility to hole mobility, in semiconductor materials such as QDs leads to

unbalanced transport of charge carriers and lower LED performance.[20] Therefore, carefully adjusting the layer thicknesses of the electron transport layer (ETL), hole transport layer (HTL), and QD layers or changing HTL/ETL layers can be utilized to control electron and hole carrier injection to individual QDs. The increase in the layer thickness of ETL and the QDs would cause a longer carrier path for the electrons and a shift of the recombination zone close to the interface between the QD and ETL layers. Decreasing the layer thickness of HTL, conversely, causes an increase in holes injected into the QD layer while still maintaining its electron-blocking property. Hence, the number of holes in the QD layer will be increased.[21] Considering these points, we adjusted first the QD layer thickness. A QD layer thickness of 20 nm led to overall better device performance, although devices with a QD layer thickness of less than 20 nm showed electroluminescence (EL) and would allow for a very thin LED architecture. We focused on two widely used electron transport materials: ZnO to ZnMgO. In this case, ZnMgO can improve charge carrier injection because of its higher conduction band than ZnO and thereby could lower the turn-on voltage.[22] Moreover, ZnMgO has lower electron mobility, which can potentially help to balance electron and hole transport in our device.[23]

The device architecture and the energy levels of the materials are shown in Fig. 2(a), depicting the valence band, conduction band, and energy bandgap; based on measurements of the QD valence band and work function (see Fig. S4) by ultraviolet photoemission spectroscopy (UPS). Figure 2(b) shows the electroluminescence emission spectrum of devices with ZnO and ZnMgO. In ZnMgO-containing QD-LED [red color in Fig. 2(b)], the main emission peak at 443 nm (deep blue/purple) and a small contribution at around 480 nm are observed. This contribution is most likely a result of a small number of charge carriers that can recombine in the TFB layer.[24] A similar contribution can be also seen in the EL spectrum of the ZnO-containing device [blue color in Fig. 2(b)]. The higher contribution in the ZnO-containing device can be a result of the higher mobility of ZnO compared to ZnMgO, therefore enabling more electrons to be injected and shifting the recombination zone toward the anode. The current density-voltage-luminance (*J-V-L*) characteristics of the fabricated devices with ZnO (blue) and ZnMgO (red) are shown in Figs. 2(c) and 2(d). The *J-V* curve of the ZnMgO-containing device shows a lower leakage current than the ZnO-containing QD-LED [Fig. 2(c)].

Finally, the QD-LED architecture with ZnO shows a maximum luminance of 6271 cd m^{-2} at 9 V, which is two times higher than the maximum luminance of ZnMgO-containing QD-LEDs (2800 cd m^{-2} at 7 V) [Fig. 2(d)]. Yet, ZnMgO-based devices show a turn-on voltage of 3 V, which is 0.5 V lower than the ZnO-based devices (3.5 V). This difference comes from the higher work function of ZnO (3.5 eV) compared to ZnMgO (3.3 eV).[23] Therefore, the injection barrier into the QD layer is lower for the ZnMgO-based devices. In addition, our I–V measurement has a step size of 0.5 V; we are therefore limited by the accuracy of the measurement and have a higher turn-on voltage difference than the work function difference of 0.2 eV. The lower turn-on voltage with the ZnMgO electron transport layer is also reported in other publications.[25] Both devices show a low decrease in current at high voltages (over 8 V) despite some indication of luminance drop, indicating good stability of the device. The ZnO-containing device obtains a maximum luminance at 9 V [blue color in Fig. 2(d)] and shows maximum current efficacy of 0.38 cd A^{-1}, and this is maintained from 4.5 V up to 9 V (Fig. S5). Overall, the additional small emission at 480 nm and the low current efficacy in the ZnO-containing devices are addressing persistent charge carrier imbalance within the device. The ZnMgO-containing device shows a higher maximum current efficacy with 0.6 cd A^{-1} but has a steep efficacy roll-off (red color in Fig. S5).

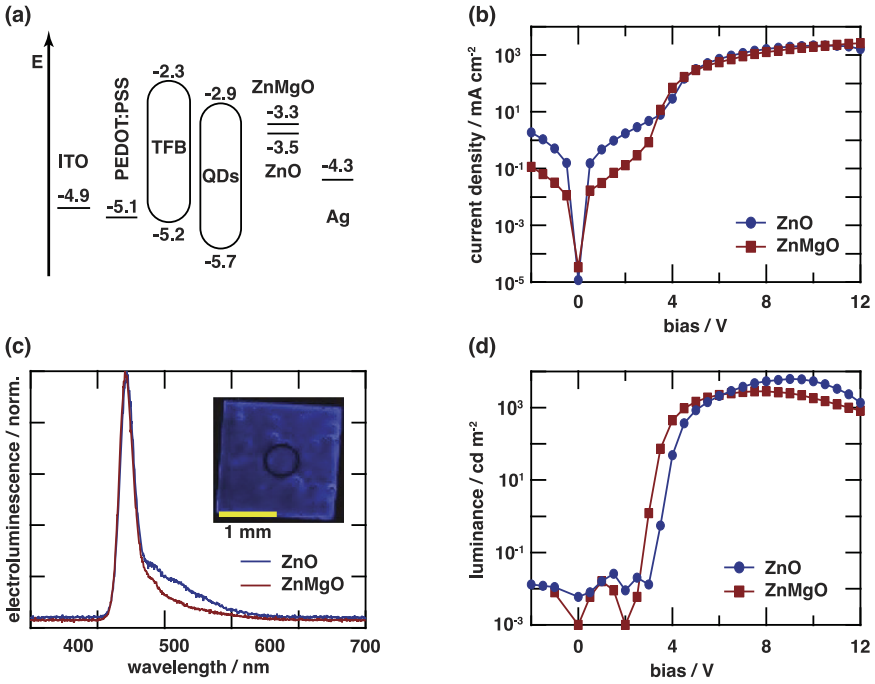

FIG. 2. (a) The energy levels of the individual layers in the QD-LED structure are vacuum aligned in this schematic and do not consider interfacial effects. (b) The electroluminescence spectrum of ZnMgO (red line) and ZnO (blue line) containing QD-LED at 7 V shows the deep blue emission, as seen in the inset, indicating a ZnO-containing QD-LED pixel under operation just after turn-on; (c) current density-voltage (*J-V*) characteristics of the QD-LEDs containing ZnMgO (red squares) and ZnO (blue circles) as ETL; (d) luminance of the same devices shows lower turn-on voltage of ZnMgO-containing device (red) and higher luminance of ZnO-containing (blue) device.

QD-LEDs are known for showing a steep efficiency roll-off that is usually caused by charge carrier imbalance. This leads to charged QDs that induce Auger recombination. Typical strategies in the literature to improve this are limiting the electron injection by adding interlayers or using different materials or ligands to improve the core/shell structure to avoid lattice mismatch.[26] Here, we attribute the steeper efficacy roll-off to the degradation due to Joule heating. The higher resistance of ZnMgO reduces the electron injection but also provides more resistive heating, which can lead to the degradation of the QDs. As a result, the loss of ligands can introduce surface traps and consequently lower the efficiency.[26]

At this point, single-carrier devices were fabricated to help understand the existing charge transport characteristics. The hole-only devices (HODs) and electron-only devices (EODs) were fabricated under the same ambient air conditions as the main QD-LEDs. HODs contain PEDOT:PSS/TFB as the hole-injection layer in the structure of ITO/PEDOT:PSS/TFB/QDs/MoO_3/Ag, while EODs are fabricated with different thicknesses of ZnMgO as an electron-injection layer in the structure of ITO/ZnMgO/QDs/ZnMgO/Ag. It is known that, in blue QD-LEDs in particular, a deeper valence band energy level introduces a higher barrier for hole injection.[27] This causes higher charge carrier imbalance and together with the higher mobility of electrons promotes the accumulation of electrons through TFB. In such cases, Mg-doped ZnO, with its lower electron mobility than ZnO, can help to suppress electron transport. In addition, it has been shown in the literature that ZnMgO in humid air can also alter the charge transport balance with the help of a decrease in hole leakage and trapped electrons.[28,29] EODs were fabricated with two different thicknesses of ZnMgO: 45 and 70 nm, with a QD layer thickness of 20 nm.

In Fig. 3, the *J-V* characteristics of HODs and EODs are shown together with power-law relations of current density (J) to the applied voltage (V). Devices could be measured up to 4 V and such a low voltage regime has characteristic regions with different slopes of exponentials, resulting in different power-law relations: Ohmic regions with a slope of 1, trap-limited space charges limited region (T-SCLC) with 1 < slope < 2, and trap-filled-limit (TFL) regions with slopes > 2. A higher voltage regime is characterized by the space charge limited region with a slope of 2 and the power-law relation of J-V^2. In Fig. 3, the overall shape of the *J-V* characteristics follows a similar trend in EOD and HOD with an indication of T-SCLC and TFL regions at low voltages.[30]

In EODs, there is a steeper increase in current density at TFL regions. In the case of the lower thickness of ZnMgO (green triangle symbols) in EODs, electron and hole currents have a crossing point at low voltages, which can indicate more balanced charge carriers.[30] Electron current is decreased (red circle symbols) to half of the hole current and there is an indication of a possible crossing point at higher voltages, i.e., higher electron than hole current. The corresponding QD-LEDs for the low and high thicknesses of ZnMgO layers are shown in Fig. 2(c) and Fig. S6, respectively. The latter, with high ZnMgO thickness, results in lower luminance.

In addition, we tested also the case of higher QD layer thickness (70 nm) for EODs and HODs. Electron and hole current showed one and two orders of magnitude difference for the low and high thickness of the ZnMgO layer (Fig. S7), respectively. The findings show the nature of charge transport in air-fabricated single-carrier devices with blue QDs. *J-V* characteristics indicate and confirm once more that charge carrier balance is highly sensitive to adjustment of each functional layer. The suppression of electron current leads to better balance in both carriers; however, too low electron current will lead to poor charge carrier balance, resulting in overall inferior performance.

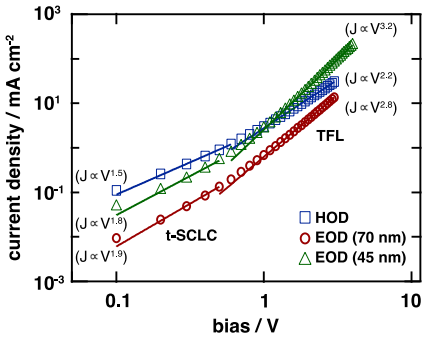

FIG. 3. *J-V* characteristics of EODs and HODs are shown in open symbols. EODs have ITO/ZnMgO/QDs/ZnMgO/Ag structure and HODs have ITO/PEDOT:PSS/TFB/QDs (20 nm)/MoO_3/Ag structure. EODs were fabricated with two different thicknesses (70 and 45 nm) of ZnMgO. The *J-V* characteristics are shown compared to HOD (squares), indicating better charge carrier balance with a low thickness of ZnMgO (green triangle symbols). Lines indicate the power-law dependence of *J-V* at high and moderate voltages for respective EODs and HODs.

In summary, we have shown the synthesis of Zn-based blue QDs and the handling of transport materials and QD material under ambient conditions from which QD-LEDs, EODs, and HODs were air-fabricated. The synthesized QDs have multi-shell structured ZnSeTe/ZnSe/ZnS (core/shell/shell) and show pure deep blue/purple emission. QD-LEDs with ZnO ETL show maximum luminance values of ~6200 cd m^{-2} with a turn-on voltage of 3.5 V that results in a current efficacy of 0.38 cd A^{-1}. Devices with ZnMgO as ETL reached maximum luminance values of ~3000 cd m^{-2} with a turn-on voltage of 3 V, i.e., at bandgap for our blue QD material, and a current efficacy of 0.6 cd A^{-1}.

Single-carrier devices show that the suppression of electron transport is crucial for better-balanced charge transport, which requires adjusting layer thicknesses of transport layers and the emitting layer. The efficiency and luminance values of QD-LEDs fabricated under inert conditions still out-perform most air-fabricated QD-LEDs; nonetheless, our study provides a step forward in air-processed blue QDs from Cd-free and less toxic materials, which can be further adapted to printing and large-area applications. To our knowledge, these are the first examples of blue QD-LEDs with a ZnSe-based QD layer, processed and measured under ambient conditions. This confirms the efficient and promising nature of these materials to be studied further and improve air-fabricated QD-LEDs.

The supplementary material contains the particle size distribution, CIE, PL, and UPS measurement of QD films, as well as additional QD-LED and single-carrier device characteristics. It also contains the experimental details of QD synthesis as well as the QD-LED and single-carrier device fabrication and characterization.

This project has received funding from the European Union's Horizon 2020 research and innovation program under Grant Agreement No. 862410 (HI-ACCURACY). The article processing charge was funded by the Deutsche Forschungsgemeinschaft (DFG, German Research Foundation) – 491192747 and the Open Access Publication Fund of Humboldt-Universität zu Berlin. We gratefully acknowledge Professor Norbert Koch for providing instrument access. The authors would like to thank Tom Lübeck for assistance in device fabrication and measurement and Michael Hengge for support with the LED measurement set-up and software for the data collection.

AUTHOR DECLARATIONS

Conflict of Interest

The authors have no conflicts to disclose.

Author Contributions

Paul Hänsch: Conceptualization (equal); Formal analysis (equal); Investigation (lead); Validation (equal); Writing – original draft (lead); Writing – review & editing (equal). **Selen Solak**: Conceptualization (equal); Formal analysis (equal); Investigation (equal); Validation (equal); Writing – original draft (equal); Writing – review & editing (equal). **Hyung Seok Choi**: Formal analysis (equal); Investigation (equal). **Yohan Kim**: Conceptualization (equal); Validation (equal); Writing – review & editing (equal). **Giovanni Ligorio**: Investigation (equal); Validation (equal); Writing – review & editing (equal). **Manuel Gensler**: Investigation (equal); Validation (equal). **Jiyong Kim**: Investigation (equal); Validation (equal). **Christine Boeffel**: Supervision (equal); Writing – review & editing (equal). **Emil J. W. List-Kratochvil**: Supervision (equal); Writing – review & editing (equal). **Felix Hermerschmidt**: Conceptualization (lead); Supervision (lead); Writing – review & editing (lead).

DATA AVAILABILITY

The data that support the findings of this study are available within the article and its supplementary material.

REFERENCES

[1]Y.-M. Huang, K. J. Singh, A.-C. Liu, C.-C. Lin, Z. Chen, K. Wang, Y. Lin, Z. Liu, T. Wu, and H.-C. Kuo, Nanomaterials **10**(7), 1327 (2020).
[2]W. Ji, T. Wang, B. Zhu, H. Zhang, R. Wang, D. Zhang, L. Chen, Q. Yang, and H. Zhang, J. Mater. Chem. C **5**(18), 4543 (2017).
[3]Q. Zhao, A. Hazarika, X. Chen, S. P. Harvey, B. W. Larson, G. R. Teeter, J. Liu, T. Song, C. Xiao, L. Shaw, M. Zhang, G. Li, M. C. Beard, and J. M. Luther, Nat. Commun. **10**(1), 2842 (2019).
[4]H. Wang, P. Zhang, and Z. Zang, Appl. Phys. Lett. **116**(16), 162103 (2020).
[5]I. Ryu, J.-Y. Ryu, G. Choe, H. Kwon, H. Park, Y.-S. Cho, R. Du, and S. Yim, Adv. Funct. Mater. **31**(34), 2102334 (2021).
[6]G. Perini, V. Palmieri, G. Ciasca, M. De Spirito, and M. Papi, Int. J. Mol. Sci. **21**(10), 3712 (2020).
[7]H. Moon, C. Lee, W. Lee, J. Kim, and H. Chae, Adv. Mater. **31**(34), 1804294 (2019).
[8]J. Ko, B. G. Jeong, J. H. Chang, J. F. Joung, S.-Y. Yoon, D. C. Lee, S. Park, J. Huh, H. Yang, W. K. Bae, S. G. Jang, and J. Bang, NPG Asia Mater. **12**(1), 19 (2020).
[9]K.-H. Lee, J.-H. Lee, W.-S. Song, H. Ko, C. Lee, J.-H. Lee, and H. Yang, ACS Nano **7**(8), 7295 (2013).
[10]Y. Yang, Y. Zheng, W. Cao, A. Titov, J. Hyvonen, J. R. Manders, J. Xue, P. H. Holloway, and L. Qian, Nat. Photonics **9**(4), 259 (2015).
[11]European Parliament and Council of the European Union, Official Journal of the European Union L174/54 (European Union, 2011).
[12]Z. Wu, P. Liu, W. Zhang, K. Wang, and X. W. Sun, ACS Energy Lett. **5**(4), 1095 (2020).
[13]H. S. Choi, S. Janietz, V. Roddatis, A. Gessner, A. Wedel, J. Kim, and Y. Kim, Nanomaterials **12**(3), 408 (2022).
[14]J. Kim, Y. Kim, K. Park, C. Boeffel, H. S. Choi, A. Taubert, and A. Wedel, Small **18**(40), e2203093 (2022).
[15]Y.-H. Won, O. Cho, T. Kim, D.-Y. Chung, T. Kim, H. Chung, H. Jang, J. Lee, D. Kim, and E. Jang, Nature **575**(7784), 634 (2019).
[16]H. Lee, Y.-H. Suh, X.-B. Fan, L. Ni, J. Yang, Y. Kim, J.-W. Jo, H. W. Choi, S.-M. Jung, D.-W. Shin, S. Lee, and J. M. Kim, J. Mater. Chem. C **10**(29), 10708 (2022).
[17]T. Kim, K.-H. Kim, S. Kim, S.-M. Choi, H. Jang, H.-K. Seo, H. Lee, D.-Y. Chung, and E. Jang, Nature **586**(7829), 385 (2020).
[18]C. Ippen, W. Guo, D. Zehnder, D. Kim, J. Manders, D. Barrera, B. Newmeyer, D. Hamilton, C. Wang, C. Hotz, R. Ma, J. K. Bin, B. Kim, K. Kim, K. Jang, J. Park, T. Lee, W. Y. Kim, and J. Lee, J. Soc. Inf. Disp. **27**(6), 338 (2019).
[19]S.-H. Lee, C.-Y. Han, S.-W. Song, D.-Y. Jo, J.-H. Jo, S.-Y. Yoon, H.-M. Kim, S. Hong, J. Y. Hwang, and H. Yang, Chem. Mater. **32**(13), 5768 (2020).
[20]N. Kirkwood, B. Singh, and M. Paul, Adv. Mater. Interfaces **3**(22), 1600868 (2016).
[21]G. Zaiats, S. Ikeda, and P. V. Kamat, NPG Asia Mater. **12**(1), 57 (2020).
[22]L. Wang, J. Lin, X. Liu, S. Cao, Y. Wang, J. Zhao, and B. Zou, J. Phys. Chem. C **124**(16), 8758 (2020).
[23]J.-H. Kim, C.-Y. Han, K.-H. Lee, K.-S. An, W. Song, J. Kim, M. S. Oh, Y. R. Do, and H. Yang, Chem. Mater. **27**(1), 197 (2015).
[24]M. G. Han, Y. Lee, H.-i. Kwon, H. Lee, T. Kim, Y.-H. Won, and E. Jang, ACS Energy Lett. **6**(4), 1577 (2021).
[25]B. Zhang, Y. Luo, C. Mai, L. Mu, M. Li, J. Wang, W. Xu, and J. Peng, Nanomaterials **11**(5), 1246 (2021).
[26]Y. Sun, Q. Su, H. Zhang, F. Wang, S. Zhang, and S. Chen, ACS Nano **13**(10), 11433 (2019).
[27]L. Zheng, G. Zhai, Y. Zhang, X. Jin, L. Gao, Z. Yun, Y. Miao, H. Wang, Y. Wu, and B. Xu, Superlattices Microstruct. **140**, 106460 (2020).
[28]S. Wang, Y. Guo, D. Feng, L. Chen, Y. Fang, H. Shen, and Z. Du, J. Mater. Chem. C **5**(19), 4724 (2017).
[29]Y. Ye, X. Zheng, D. Chen, Y. Deng, D. Chen, Y. Hao, X. Dai, and Y. Jin, J. Phys. Chem. Lett. **11**(12), 4649 (2020).
[30]S.-K. Kim, H. Yang, and Y.-S. Kim, J. Appl. Phys. **126**(18), 185702 (2019).